京都大学防災研究所年報 第 53 号 B 平成 22 年 6 月
Annuals of Disas. Prev. Res. Inst., Kyoto Univ., No. 53 B, 2010

Assessment of Spatially-Distributed Sediment Budget and Potential Shallow Landslide Area for Investment Prioritization in Sediment Control of Ungauged Catchment: A Case Study on the upper Citarum River, Indonesia

APIP*, Kaoru TAKARA, Yosuke YAMASHIKI, and Agung Bagiawan IBRAHIM**

*Graduate School of Urban and Environment Engineering, Kyoto University
** Research Centre for Water Resources, Department of Public Works, Indonesia

Synopsis

A few internal locations of the catchment are critical and responsible for high amount of soil losses due to surface soil erosion and shallow landslide events. Implementation of best management practices is required in those critical sediment source prone areas of the catchment for controlling the soil losses. Identification of these critical areas is essential for the effective and efficient implementation of catchment management programs. In this study a physically-based distributed hydrological-geotechnical model was developed for an upland catchment (2,310 km^2) and aimed as an assessment tool for identification and prioritization of critical internal locations (sub-catchment scale) to develop an effective management plan. The model consists of two primary components: hillslope sediment-runoff, it considers soil detachments by raindrops and surface runoff; and a stochastic slope instability predictions. Daily streamflow and sediment yield data (2001–2004) as well as the spatial patterns of documented historical landslides (1985–2008) were used for the model verification and application. Critical sub-catchments were identified on the basis of spatially-distributed sediment yield rates and predicted shallow landslide probability. The study revealed that the proposed distributed model could successfully be used for identifying and prioritizing critical internal ungauged locations of the catchment for management purposes.

Keywords: sediment control, soil erosion, slope instability, Citarum River.

1. Introduction

The upper Citarum River catchment (2,283 km^2), West Java, Indonesia was selected as a study area. At the outlet of the upper Citarum River, the Saguling Reservoir was constructed in 1986. The main purpose of this construction is to be a main source of hydropower in Java Island, also of water supply to freshwater fisheries and agriculture. Because of its position as the upper reservoir, most of the gross storage has been already filled with the large amount of sediment materials brought by flood events. If the sedimentation keeps happening without any prevention and controlling actions, it will restrict reservoir functions and its lifetime. Herein, the condition of upper river catchment is an important factor in controlling the water balance, soil erosion, and sedimentation rate.

The upper Citarum River catchment is one of the persistently active landslides occurring in Indonesia. The floods triggering landslides are hit almost in every year and caused extensive damages. Hydrologic characteristics have been changed by land degradation (Agus *et al*., 2003), as a result, flood, debris flow and others landslide types are very frequent during the rainy season. The soils derived from volcanic tuff are easily erodible and prone to landslides. Hillslopes erosion is also a serious problem in this upper area where hillsides are steep. Shallow landsliding as a form of mass movement and surface soil erosions are the main source of catchment sediment yield. Therefore, there was an urgent need to devise countermeasure actions.

Numerous studies have indicated that, for many catchments, a few critical locations are responsible for high amount of the pollution (Lin *et al*., 2008; Dickinson *et al*., 1990). Therefore, it is better to begin management measures from the most critical internal location such as at sub-catchment scale, which makes it mandatory to prioritize the sub-catchment available. The investment area prioritization is thus the ranking of different critical sub-catchments of a catchment according to order in which they have to be taken up for structural or non structural measures. Structural measures can be employed here: vegetative filter, wet pond, reservoir, and land use scenario.

For sediment rate reduction programs, an effective control of soil losses requires implementation of best management practices (BMPs) in critical sediment source prone areas of the catchment. It can be enhanced by the use of physically-based distributed model that can be utilized as an assessment tool in both identifying most vulnerable sediment source prone areas and selecting appropriate management practices.

The research works on identification of critical areas inside a catchment on the basis spatially-distributed sediment yields and shallow landslide potential areas has not appeared much in the literature. Keeping this fact in mind, the current study analyzed hydrological-geotechnical and sediment transport-tation processes at the upland catchment through a modeling system to understand the spatial dynamic sediment yield and transportation, to identify the critical areas according to the level of sediment yield and susceptibility of shallow landslide areas, as well to guide decision making in strategic design related to sediment-runoff and slope instability control. Since there is has the scarcity of gauging stations for surface soil erosion and landslide monitoring, a distributed model is most suitable tool for the estimation of sediment-water balance and slope stability at internal ungauged locations of the upper Citarum River catchment.

A physically-based distributed hydrological-geotechnical model has been developed to consider multiple sources of sediment transport, namely soil detachment by raindrops, soil detachment by overland flow, and shallow landslides which is stochastic in nature. Linking this model outputs and various BMPs scenario algorithms is very useful for making a design of control strategy in controlling sediment-runoff and slope instability. The impact of spatial heterogeneity of sediment transport and varying the spatial scale of target locations on cost effectiveness can be also examined.

2. Study Area

The upper Citarum Catchmet with Saguling Reservoir as the outlet is located in mountainous area of the West Java Province, and total area of the catchment is the 2,310 km^2 lying between 600 to 3000 m. Geographically, the area is lies off $107^o26'E$-$107^o95'E$ and $6^o73'S$-$7^o25'S$ (Figure 1a). The average of slope gradients by using a DEM 90 m resolution range from 0.01^o in the central area to 31.15^o in northern and southern parts.

The current water related problems are floods and landslides in the wet season and droughts in the dry season. The hillslopes areas of this region have been periodically exposed to hazards from shallow landslides and debris flows. Most of those landslides were triggered by a series heavy rainfall. The climate conditions are characterized by tropical monsoon

with two distinct wet and dry seasons. A series of data from BMG specifying that high amount of rainfall is at the beginning of November-December followed by a second peak in March-April, results from the westerly monsoon. The rainfall amount then quickly slackening down in May-October due to dry season as results from the prevailing easterly monsoon. Annually rainfall of the area varies from 1500 mm up to 4000 mm, with almost 80% falling between November and April.

The nature of vegetation on the land surface influences the hydrologic and slope stability conditions. The land use information was produced from LANDSAT7/ETM+ (30 m resolution) satellite images and verified by field investigations. Twelve land use type classifications were applied for land use in 2002. Below 800 m, the land use is mainly covered by paddy fields and settlement areas. At the intermediate altitudes and the steep slopes the land use is mainly farmland (cultivation of annual or tree crops), orchards (perennial trees), forest, grass, and shrub. The urbanized areas also covering the steep slopes although are relatively small and concentrated only in several spot areas which are high susceptibility to landsliding.

The geological formation consists mainly of old quaternary volcanic product with some miocene sedimentary facies, granit, granodiorite, diorite, alluvium, pleistocene volcanic facies, and miocene limestone facies (Takeuchi *et al*., 1995). Due to the influence of the active volcano, the types of soils in the study area are varies and underlined complex. Based on the digitized soil map and derived soil properties provided by FAO-UNESCO, the humic and ochric andosol soils mainly lay on the mountainous area in which was influenced by volcanic eruption. Latosol is stretched along the lembang fault, and alluvial is occupied along side of the river valley. The spatial distribution of soil thickness in study catchment required for performing the hydrological model and the infinite slope stability model is range from less than 10 cm to 150 cm.

The catchment is owing to the limited spatial coverage of ground-based rain gauges and unavailability of real-time rainfall data. The rainfall was measured by using 17 daily rain gauges and only one station available there for automatically recording rainfall intensity. Water level recorders were installed to measure streamflow discharge which are approximated using rating curves. This includes one sediment discharge gauge located at the Inlet of Saguling Reservoir (Nanjung Station). The locations of those hydrological and meteorological stations are shown in Figure 1b.

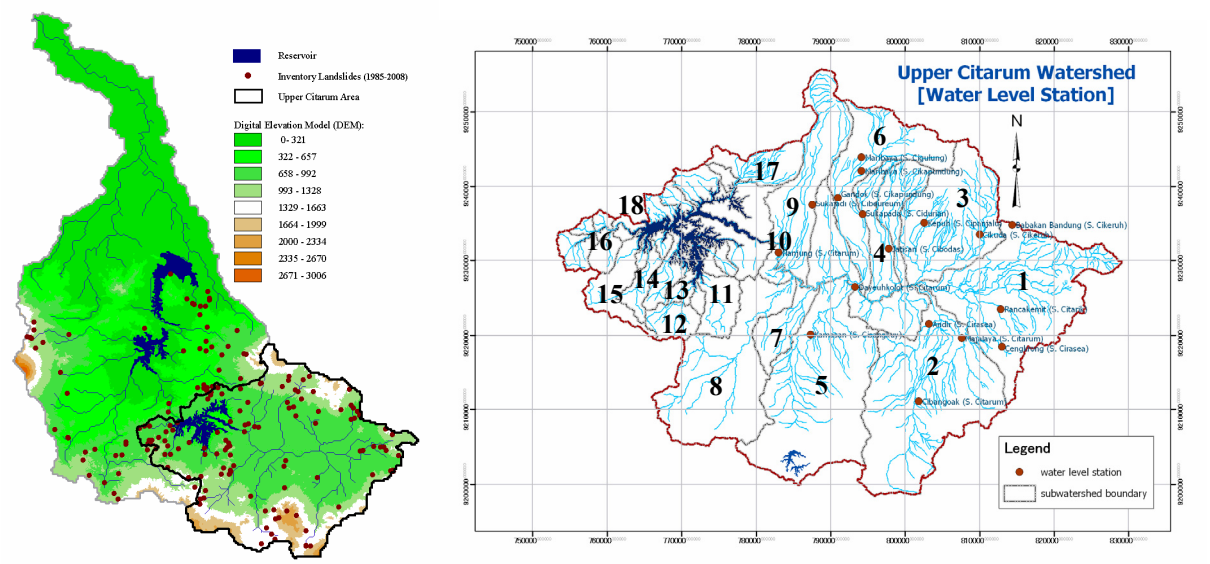

Fig 1. (a) Location of the upper Citarum River catchment over the whole DEM Citarum River watershed. The red points indicate the locations of landslides as inventoried by the Geological Agency of Indonesia, and (b) Sub-catchments (shown by a number) in the upper catchment associated with water level stations.

3. Original Distributed Rainfall-Sediment-Runoff Model

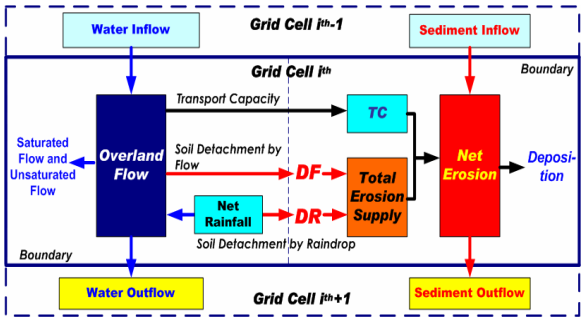

Fig. 2 Schematic diagram of the physically-based distributed sediment-runoff model within a grid-cell scale.

An original distributed rainfall-sediment-runoff model is constructed upon a distributed rainfall-runoff model (Tachikawa *et al.*, 2004). The model simulates three lateral flow mechanisms including (1) subsurface flow through capillary pore, (2) subsurface flow through non-capillary pore, and (3) surface flow on the soil layer. These three flow processes are represented by the following single set of stage-discharge relationships (Equation 1):

$$q=\begin{cases} v_m d_m (h/d_m)^{\beta}, & o \le h \le d_m \\ v_m d_m + v_a (h-d_m), & d_m \le h \le d_a \\ v_m d_m + v_a (h-d_m) + \alpha (h-d_a)^m, & d_a \le h \end{cases} \quad (1),$$

$$v_m = k_m i \ , \quad v_a = k_s i \ , \quad k_m = k_s / \beta \ , \quad \alpha = \sqrt{i}/n \ ,$$

$$d_m = D\theta_m , \quad d_a = D\theta_a$$

where q is discharge per unit width; h is water depth; i is the topographic gradient; k_m is the saturated hydraulic conductivity of the capillary soil layer; k_s is the hydraulic conductivity of the non-capillary soil layer; d_m is the depth of the capillary soil layer; θ_m is the fraction of maximum volumetric water content in the capillary pore (= 0.25), d_a represents the depths of the capillary and non-capillary soil layers, θ_a is the fraction of maximum volumetric water content in the capillary and non-capillary pores (= 0.75); D is a soil depth; β is the exponent constant of unsaturated flow, v_m and v_a are the flow velocities of unsaturated and saturated subsurface flows, respectively, n is the Manning's roughness coefficient which varies in land use type, and m is 5/3.

Soil transport simulation processes was included onto the above mentioned rainfall-runoff model (Apip *et al.*, 2008). Soil detachment processes at interrill and rill are implicitly simulated as raindrop splash and surface flow detachment, respectively (Figure 2). The empirical equation of soil detachment by raindrops d_r is given as

$$d_r = \mu k k_e = \mu k 56.48 r \quad (2),$$

where μ is the soil erodibility; k is a parameter (= 1.0); and k_e is the total kinetic energy of raindrop (J/m^2/hr). The concept of sediment transport capacity was used to determine soil detachment or deposition by surface flow d_f (Foster, 1982):

$$d_f = \alpha (T_c - c) h_{ws} \quad (3),$$

where α is a proportionality coefficient; h_{ws} is the surface flow depth; and T_c is the maximum sediment concentration transport capacity (kg m^{-3}), which determines soil erosion (when $T_c > c$) or deposition (when $T_c < c$). In the present work, the sediment transport capacity was calculated based on the Unit Stream Power (USP) theory (Yang, 1996), is expressed as

$$T_c = \log\{i + j \log((vi - v_{critical}\, i)/\omega)\} \quad (4),$$

where vi is the unit stream power (where v is the surface flow velocity calculated by Equation 1 and i is the slope gradient) and $v_{cr}i$ is the critical unit stream power required at incipient motion (= 0.002 m s^{-1}), in which

$$i = 5.435 - 0.386 \log(\omega d_{50}/\upsilon) - 0.457 \log(U^*/\omega)$$

$$j = 1.799 - 0.409 \log(\omega d_{50}/\upsilon) - 0.314 \log(U^*/\omega)$$

$$\omega = F\left[g d_{50} \left(\frac{\rho_s}{\rho_w} - 1 \right) \right]^{1/2}$$

where

$$F = \left[\frac{2}{3} + \frac{36\upsilon^2}{(\rho_s/\rho_w - 1) g d_{50}^3}\right]^{1/2} - \left[\frac{36\upsilon^2}{(\rho_s/\rho_w - 1) g d_{50}^3}\right]^{1/2}$$

where vi is the unit stream power (where v is the flow velocity and i is the slope gradient), $v_{critical}\, i$ is the critical unit stream power ($v_{critical}$ is the critical flow velocity), ω is the sediment fall velocity calculated by Rubey's equation, ρ_s is the sediment particle density, ρ_w is the water density, g is the specific gravity, d_{50} is the median grain size (mm), and υ is the kinematic viscosity of the water. $U^*(=\sqrt{g\, i\, h_s})$ is the average shear velocity. There are three model parameters that have to be calibrated μ, α, and D_{50}.

4. Landslide Susceptibility

The method combines the following two model outputs necessary for identifying where and when shallow landslides may potentially occur in the catchment: (1) the time-invariant spatial distribution of areas susceptible to slope instability map, for which the river catchment is divided into stability classes according to the critical relative soil saturation; this output is designed to portray the effect of quasi-static land surface variables and soil strength properties on slope instability; and (2) a produced map linked with spatiotemporally varying hydrologic properties to provide a time-varying estimate of susceptibility to slope movement in response to rainfall. The proposed hydrological model predicts the dynamic of soil saturation in each grid element. The stored water in each grid element is then used for updating the relative soil saturation and analyzing the slope stability. A grid of slope is defined to be unstable when the relative soil saturation becomes higher than the critical level. The following explanation is the basic equations use in the slope stability model.

Shallow Landslide Susceptibility Map Using a Factor of Safety

Engineering geologists often use the relationship between shear stress (the component of stress that operates in the down-slope direction, τ) and shear strength (the properties that resist shear stress, i.e., cohesion + normal stress) to carry out a slope stability analysis. The ratio of shear strength to shear stress is called the factor of safety (FS). For modeling shallow landslides the simplified case of a planar failure on an infinite slope is generally accepted and the FS is calculated by Equation 5 (Montgomery and Dietrich, 1994). When this ratio is greater than 1.0, shear strength is greater than shear stress and the slope is considered stable. When this ratio is close to 1, shear strength is nearly equal to shear stress and the slope is unstable.

$$FS = \frac{c^* + \cos\theta\,[1 - r_u]\tan\phi}{\sin\theta};\begin{cases} c^* = \dfrac{c}{\rho_s\, g\, h} \\ r_u = \dfrac{h_w\, \rho_w}{h\, \rho_s} \end{cases} \quad (5),$$

in which c is the total cohesion (c_r+c_s), c_r and c_s is the effective root and soil cohesion; ϕ is the effective angle of internal of soil; h is the soil depth; h_w is the saturated depth; θ is the slope angle; ρ_s is the mass density of soil at field moisture; ρ_w is the weight density of water. Most of are can be spatially variable but it is assumed that only m (=h_w/h) is time-varying, therefore, the factor of FS is a function of m. Assuming that the value of every term in Equation 5, except for m, is known or can be estimated for each local area/grid, a critical relative saturated depth for a grid m^c can be determined, where m^c_i=FS_i^{-1}(1) (Equation 6).

$$m^c = \left(\frac{h_w}{h}\right)^c = \frac{\rho_s}{\rho_w}\left(1 - \frac{\tan\theta}{\tan\phi}\right) + \frac{c}{h\, \rho_w\, g \cos\theta \tan\phi} \quad (6).$$

Based upon the concept of critical soil saturation, three slope stability classes can be defined:

1. Theoretically always stable which is expressed by

$$\tan\theta < \tan\phi\left(1 - \frac{\rho_w}{\rho_s}\right) + \frac{c}{h\, \rho_s\, g \cos\theta} \quad (7).$$

2. Theoretically always unstable, is expressed by

$$\tan\theta \geq \tan\phi + \frac{c}{h\, \rho_s\, g \cos\theta} \quad (8).$$

3. Potentially stable or unstable, predicted by Equation (5)

Land surfaces theoretically always stable are those predicted to be stable even when saturated as well as slope elements theoretically always unstable are those predicted to be unstable even when dry condition. There are four model parameters that have to be calibrated c_r, c_s, ϕ, and ρ_s.

Generate and Extract Susceptibility Maps

To asses the critical sub-catchment on the basis of susceptible shallow landslide area, the Generalized Likelihood Uncertainty Estimation (GLUE) concept is adopted and incorporated into the above deterministic slope stability model to generate 10000 landslide susceptibility maps. The procedures (Figure 3) include a number of steps:

1. Generate a probabilistic distribution and sampling the parameter space of each model parameters using 10000 times of Monte Carlo simulation technique
2. Measurement of model performance
3. Define the criteria for acceptance or rejection of model results.

For each simulation, when the *FS* value for a grid less than 1.0 is defined as shallow landslide would occur, otherwise, stable. The long-term spatial pattern of recorded landslide locations (1985-2008) is overlaid to each susceptibility map. Two objective functions are used to measure the model performance for each susceptibility map namely success rate in predicted unstable grids (SRUG) and success rate in predicted unstable grids associated with success rate in predicted stable grids (SRUG+SRSG) (see Figure 3 for equations). Accordingly, the cumulative probability of predicted landslide and mean *FS* for each grid could be extracted; thus a relative risk measure for landslide potential can be made. The probability of landslide potential on the basis of slope instability index qualitatively is defined as extremely low, low, moderate, high, and extremely high.

5. Space-Borne Real-Time Rainfall Estimates

High temporal and spatial resolution rainfall estimates are required for sediment-runoff and shallow landslide predictions. The use of a rainfall product derived from satellite images is one of the alternatives for poorly gauged areas such as the upper Citarum Catchment. The main data set used in the present study was the CMORPH global rainfall product prepared by the Climate Prediction Center of the National Oceanic and Atmospheric Administration (NOAA), USA.

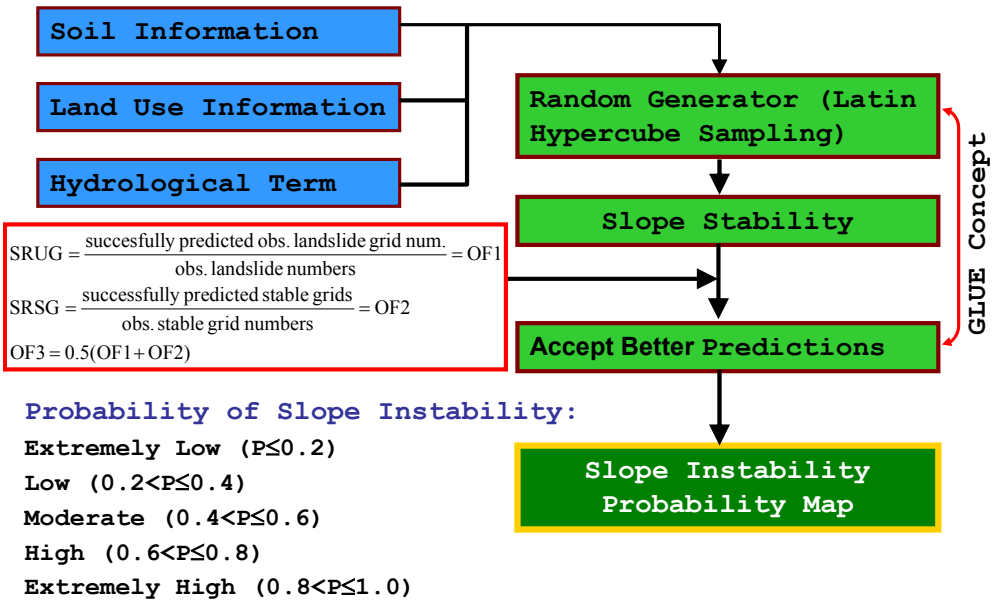

Fig. 3 the stochastic procedure to generate landslide susceptibility areas and predicted landslide probability.

This rainfall product has fine temporal and spatial resolutions and was developed using a new satellite-based technique and algorithm for rainfall estimation called "CMORPH", short for the Climate Prediction Center morphing method. More detail on the CMORPH method that produces satellite-based global precipitation estimates and its validation can be found in Joyce et al. (2004).

The entire CMORPH record at a grid resolution of the 0.07277 degrees lat/lon (8 km at the equator) and regional domain 60° N-60° S was introduced in December 2002 and is available on the NOAA-CPC web site (http://www.cpc.ncep.noaa.gov/).With regard to spatial resolution, although the rainfall estimates are available on a grid with a spacing of 8 km, the resolution of the individual PMW sensors associated satellites is coarser than that which more on the order of 12 x 15 km. The finer resolution is produced via interpolation. A near real-time version of the half-hourly CMORPH data product with more timely estimates called "QMORPH estimates" has been used in this study. The CMORPH satellite images were processed using ENVI and ER Mapper image-processing software, and the output datasets were then formatted to GIS format and resampled to the same grid resolution and projection system as the data input to the hydrological–geotechnical model.

Evaluation of the hydrological model performance through calibration and validation of a hydrological response was carried out considering long-term and short-term simulations. The years 2001 and 2004 were selected as the calibration and validation periods. Discharge data from six water-level stations at the gauged sub-catchments (see Figure 1b) were used to calibrate and validate the simulated streamflow discharges. The rainfall recorded at 18 daily rainfall stations, distributed in and around the catchment, was utilized to account for the distribution of rainfall. However, only one hourly rain gauge was available, daily rainfall data were disaggregated to hourly values using an approach derived from the analysis of various temporal rainfall patterns of heavy rainfall events at the automatic rain gauge of BMG Station. The total rainstorm event for different time duration during the period 1986-2004 was analyzed. We found that heavy 4-hour rainfalls as the highest density of total rainfall events. The average temporal distribution pattern of heavy 4-hour rainfalls was used as a simple model for generating hourly rainfall series from a daily rainfall (Figure 4). The rain tends to begin from 14:00 local time and continued for 4 hours. Assuming the same proportional distribution for the general temporal rainfall pattern as at BMG Station but conserving the measured volumes as well as considers the tropical rainfall characteristics in Sumatera and Java islands (Wu et al. 2003), the rainfall pattern within a day at a daily rain gauge was achieved by distributing the rainfall to an hourly rainfall sequence. Then the hourly rainfall values were spatially interpolated. Herein, the Thiessen polygon method was used to estimate the spatial rainfall distribution in the catchment. The interpolated and disaggregated data standardized to GIS format then served as the input for the space- and time-varying hydrological model calibration and validation.

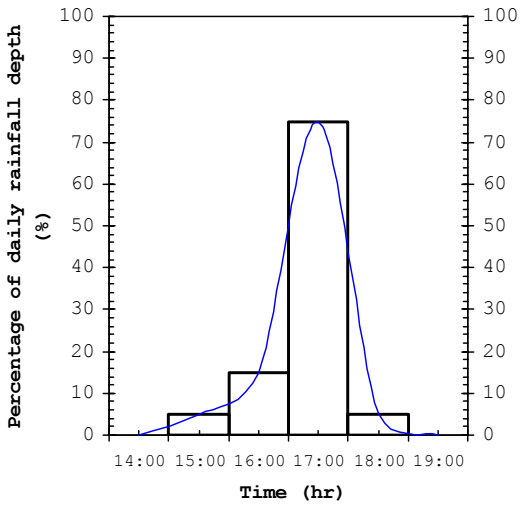

Fig 4. Transformation from a daily rainfall to a hourly sequence in the upper Citarum Catchment.

6. Observed Sediment Yield and Past Landslide Events

The upstream area of Citarum Catchment is surrounded by many mountains, such as Mount Wayang, Mount Calancang, Mount Patuha, Mount

Malabar, Mount Tangkuban Perahu, etc. Therefore, the upstream land area is steeply sloping. This characteristic brings large tendency to soil erosion and sliding if the land lacks in well covering vegetation.

To give a real description of erosion tendency in Citarum upper area, a series of data in two time periods is compared. The monitoring station is at Nanjung, which is located right at upper course of Saguling Reservoir. With annually averaged flow of 92.3 m^3/s, the upper Citarum stream monitored at Nanjung is quite heavy. The flow brought about 1.05 million ton per year of suspended sediment in 1981 to 1982 period. With less covering vegetation on the upstream area, it is noted that the sedimentation rate had increased to 4.80 million ton per year in 2004. In short, there is five times rising of sedimentation rate in almost 20 years period.

The characteristics of landslides in study region can be classified into two types with regard to depth and speed of landslide movement from the aspect of risk: first, is deep and slow landslides, relatively safe for people, no causalities since they allow evacuation even during motion. However, landslide movement can be enough to destroy houses and other buildings with large damaged area, and second, is shallow and rapid landslides, are dangerous especially when many landslides will occur during the same triggering rainfall event, those causing causalities and large numbers of infrastructure damaged. The speed in this type of landslide is very rapid with rock, soil, and debris flows.

As an example, three significant debris flow events occurred, those categorized come from rapid and shallow landslides triggered by heavy rainfall and produced much sediment yield during April 2004 and March 2008 as follows:

- Landslide disaster in West Java at Cililin, Walahir village on 21 April 2004 that caused at least 15 peoples dead, 43 houses collapsed and heavy damaged, 60 Ha of paddy fields have been swept away by the landslides. This landslide mainly was due to heavy rainfall, steep slope, high weathering products, and land-use changed.
- Landslides disaster in West Java at Pangalengan and Cikembang Villages on 15-16 March 2008 that caused 2 residents were believed to have died and 48 houses buried by the landslides. This landslide mainly was caused by heavy rainfall and steep slope.

7. Evaluation of the Model's Performance

Streamflow Discharge and Sediment Yield

The performance of the distributed hydrological model in reproducing observed streamflow and sediment discharges using the calibrated model parameters was evaluated. In principle, the spatial and temporal variations of soil saturation for all internal locations of the catchment should be considered as the target model output for the calibration process. However, spatial and temporal observations were not available for this study region. Therefore, a degree of calibration or adjustment of the parameter values was conducted only to reproduce the observed streamflow and sediment discharges as accurately as possible. The hydrological model includes eight parameters that should be adjusted through a calibration procedure. In this study, only the Manning Roughness coefficient is spatially distributed according to the land-use, whereas other parameters are spatially uniform over the gauged sub-catchments. The physical meaning of each parameter range value was obtained from the literature. The upper and lower bounds of the parameter spaces are given in Table 1. Adjustment of final parameters was conducted by performing Monte-Carlo-type simulations on the basis of best model performance. The physically based distributed model was run using a horizontal 90-m square grid resolution. The DEM was provided from HydroSHEDS global topographic–hydrographic information (http://hydrosheds.cr.usgs.gov).

Observed and simulated hydrographs and these cumulative sediment yields at Nanjung Station are summarized in Figure 5, in which each panel shows the result of calibration and validation. Using the same parameters from the

Table 1 Parameter spaces of the sediment-runoff model used in the model evaluation.

Model Parameter	Description	Parameter Space	Reference
n [$m^{-1/3}$ s]	Manning roughness coefficient for six types of land-use (forest, farmland, orchard field, urban land, paddy field, and river)	0.01-1.50	Morgan *et al*., 1998; Sayama *et al*., 2003; Kojima & Takara, 2003
k_a [mm s^{-1}]	Hydraulic coefficient of saturated soil layer	0.001-0.16	Assumed*
d_a [mm]	Total non-capillary and capillary soil layer depth	100.-500.	Assumed*
d_m [mm]	Capillary soil layer depth	50.-250.	Assumed*
β	Exponent constant of unsaturated flow	2.0-10.0	Assumed*
d_{50} [mm]	Median of sediment grain size	0.01-0.20	Measurement
μ [g J^{-1}]	Soil detachability of raindrop erosion	1.50-3.50	Morgan *et al*., 1998
α	Efficiency factor of soil detachment/deposition by flow	0.90-1.00	Assumed

* Parameter range covers the calibrated values defined by the previous studies (Tachikawa *et al*., 2004; Sayama *et al*., 2003).

Table 2. Parameter ranges used for slope stability model calibration

Model Parameter	Description	Parameter Space
c [kPa]	Soil cohesion	1-11
ϕ [deg]	Internal angle friction	5-34
ρ_s [kg m^{-3}]	Soil density	1300-1415

calibration period, the hydrological model was run for the validation period. The results depicted in Figure 5 indicate that after calibration, the model yielded comparable results with respect to long-term daily streamflow and sediment discharges. The model generally predicted the overall shape of hydrographs and cumulative sediment yields reasonably well. However, the model tended to produce overestimates, especially for low streamflow discharges. The performance of the streamflow model was evaluated using the Nash–Sutcliffe coefficient of efficiency (NSE). The NSE values for the calibration and validation periods were 0.752 and 0.617, respectively, indicating that the model can effectively predict hydrological responses. The model was in a reasonable way for reproducing observed sediment yield at Saguling Dam inlet, in which the flows brought about 1.0-4.0 million ton/year.

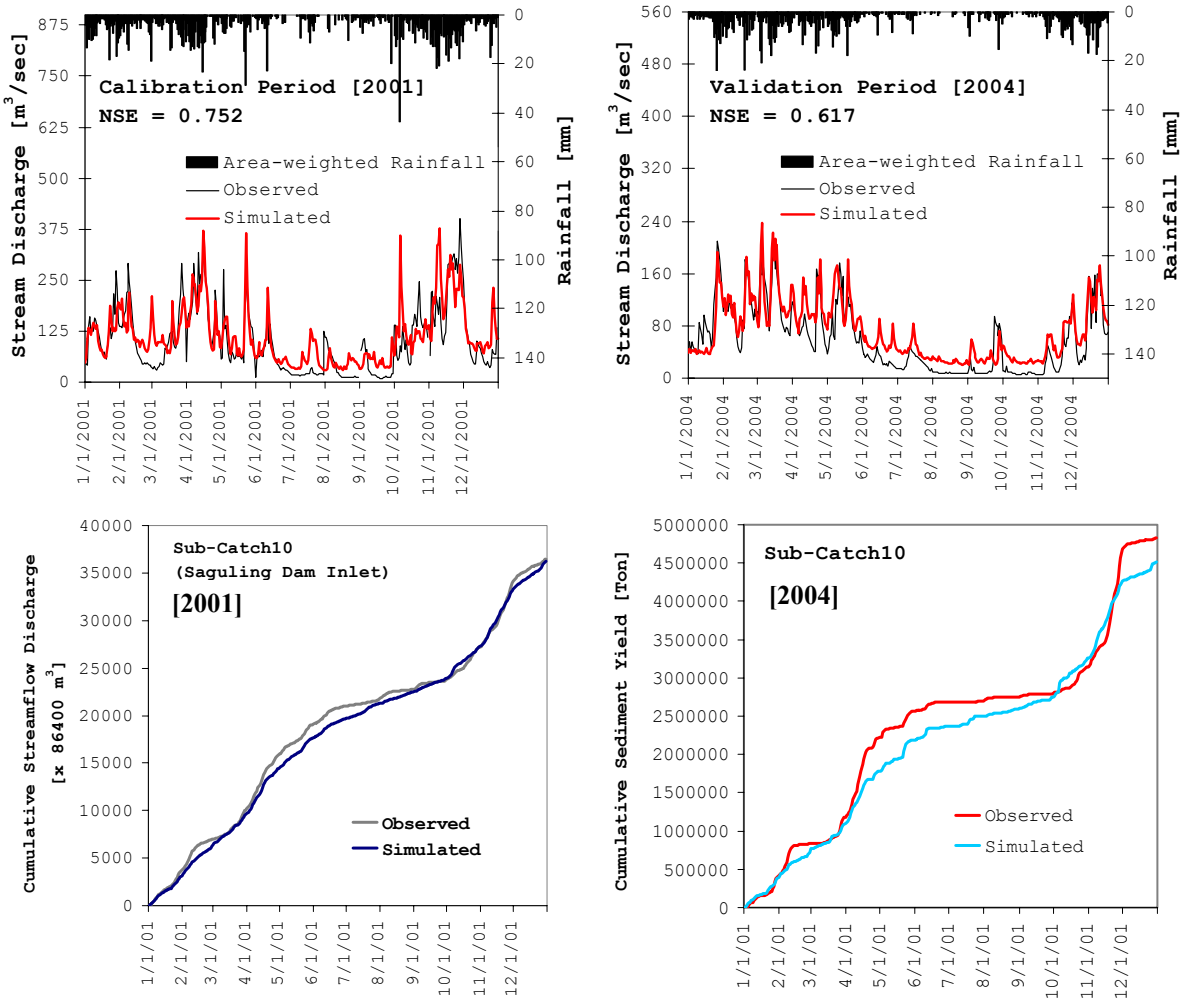

Fig. 5 stream flow and cumulative sediment yield model performance for calibration period (left column) and validation period (right column). Streamflow and sediment discharges were evaluated at the catchment outlet.

Integrate Susceptibility Maps

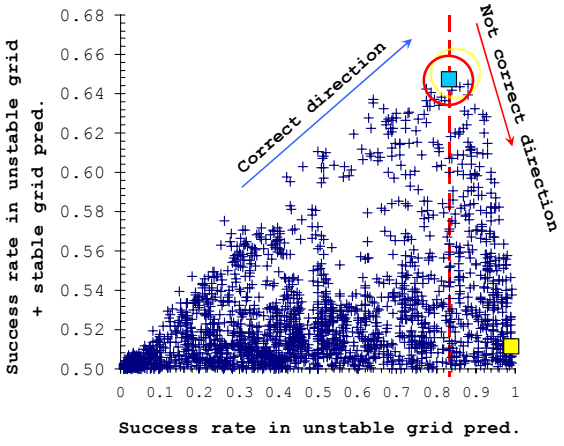

Fig 6. The scatter plot of OF1 againt OF3-derived efficiencies for the 2067 runs.

Adjustment of geotechnical parameters was conducted by performing Monte-Carlo-type simulation (MCS) technique and adopted GLUE concept. Initial estimates for feasible ranges of those slope-stability model parameters were estimated on the basis of field and laboratory measurements as well as soil type and soil thickness maps (Table 2).

Following GLUE, we set a reference value for model performance (OF3 ≥ 0.50) to define the behavioural simulations. There are 2067 susceptibility maps belong to the applicable simulations. Here we demonstrate the advantage of using two objective functions; OF1 and OF3 (see Figure 3) to measure model performance and problems in retrieving optimal model outcome. The 2067 top values of model performance derived from OF3 are plotted against the OF1 (Figure 6). A

dome-shape distribution is shown between the two objective functions. OF3-derived performance increases together with OF1-derived performance at the beginning. However, when OF3-derived performance reaches a best prediction (0.64) and starts to decrease but OF1-derived efficiencies keep increasing until its best prediction (1.0). The result suggests that OF3-derived performance enables to reduce over prediction.

For probability analysis, we overlap maps and take mean for *FS* values in each grid for the 2067 better predictions. On the other hand we calculate the occurrence probability of $FS < 1.0$ for each grid in the 2067 runs to quantify predicted shallow landslide potential. For each grid we have a mean *FS* value and an occurrence probability for shallow landslide potential (Figure 7).

[a]

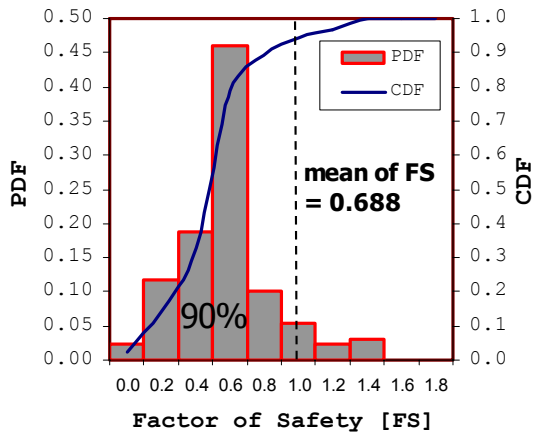

[b]

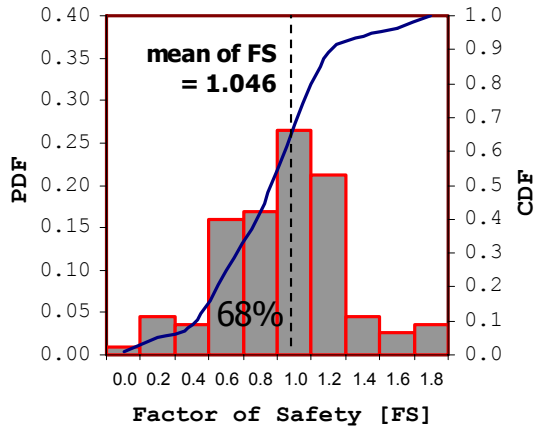

[c]

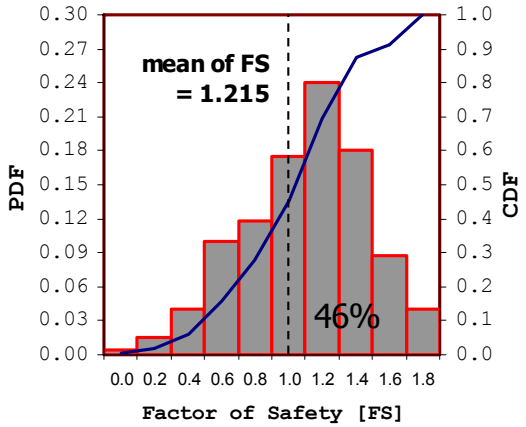

Fig. 7 Probability functions and their cumulative probability of the *FS* values in the three example grids with different mean *FS*: unstable [a]; moderate [b]; and stable [c].

Figure 8 shows the integrated landslide probability map derived from the better 2067 simulations and its spatial distribution of mean *FS* with OF3 equal 0.50. Figure 8 demonstrates the patterns of areas are predicted to be susceptible to shallow landslide as described above along with the general pattern of observed landslide sources. The model reproduced several of the principle clusters in the observed pattern, notably the clusters along an escarpment in the western, southern, eastern, and northern sectors of the catchment. The percentage of catchment area used to simulate the dynamic of susceptible areas to shallow landsliding in response to a rainfall event amounted to 32.1% (636,318 grids).

Two types of error appeared in the estimated time-invariant slope-stability classes map: (1) some grids were predicted as theoretically always stable, but past landslides were mapped in those grids, especially in the northern part of the study region; (2) some grids were characterized as the zone of instability slope, but no scars were observed there. Such errors are typically caused by inaccuracies in model topography. In steep terrain, the 90-m grid DEMs provided by HydroSHEDS for particular internal locations still do not capture the local slope steepness that controls shallow landsliding. Consequently, the model did not represent local topographic controls on potential shallow landsliding.

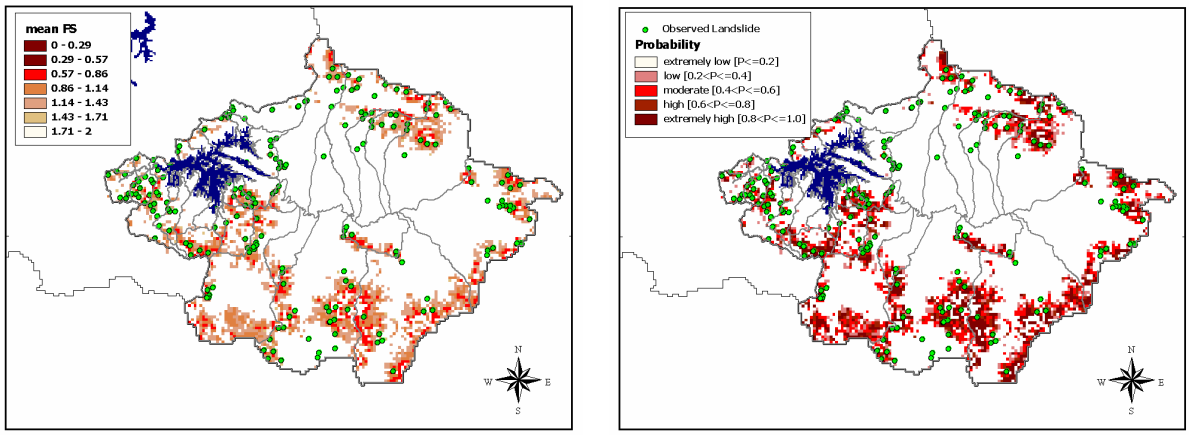

Fig. 8 The mean FS (left column) and integrated landslide probability map (right column) inside the best prediction zone (OF3 values = 0.64) overlaid with a spatial distribution of observed landslide locations.

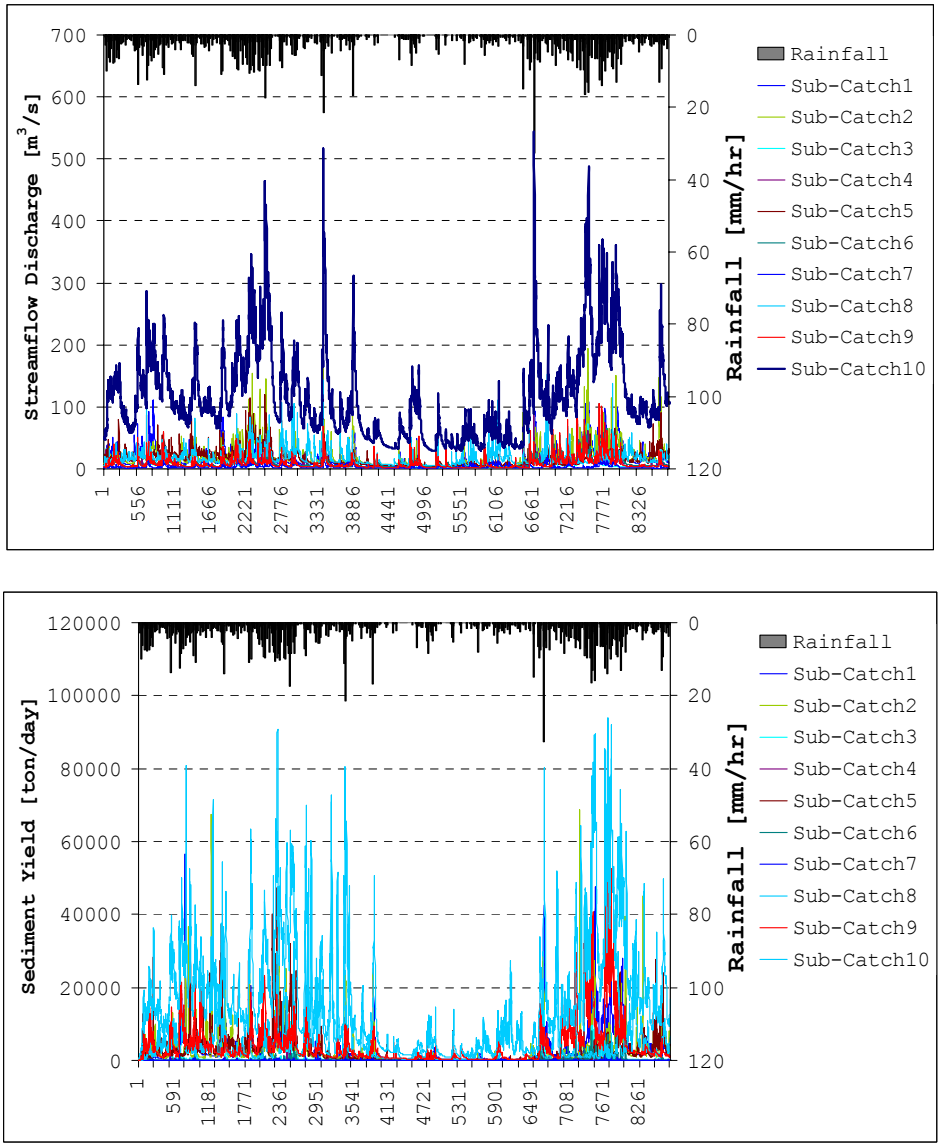

Fig. 9 Hourly simulated runoff (upper figure) and sediment yield (lower figure) for main river and each sub-catchment.

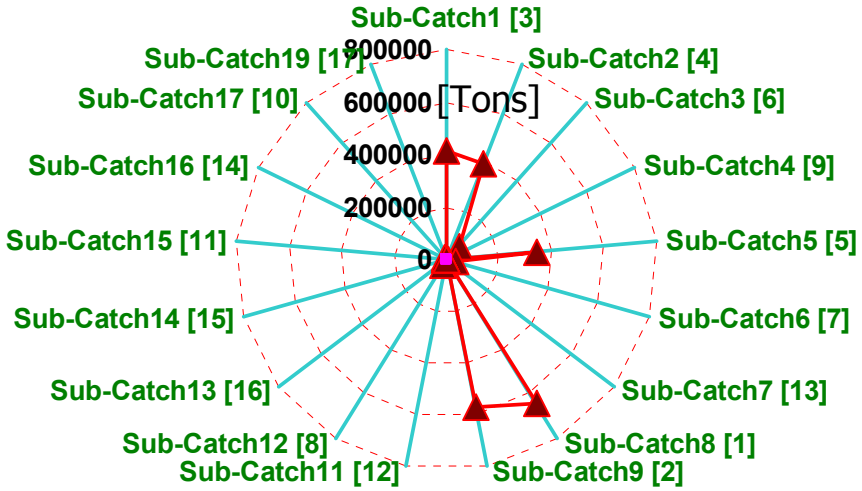

Fig. 10 Model output for identification of the critical sub-catchment for soil erosion in the upper Citarum Catchment. The ranking of critical sub-catchments is shown by the numbers inside bracket.

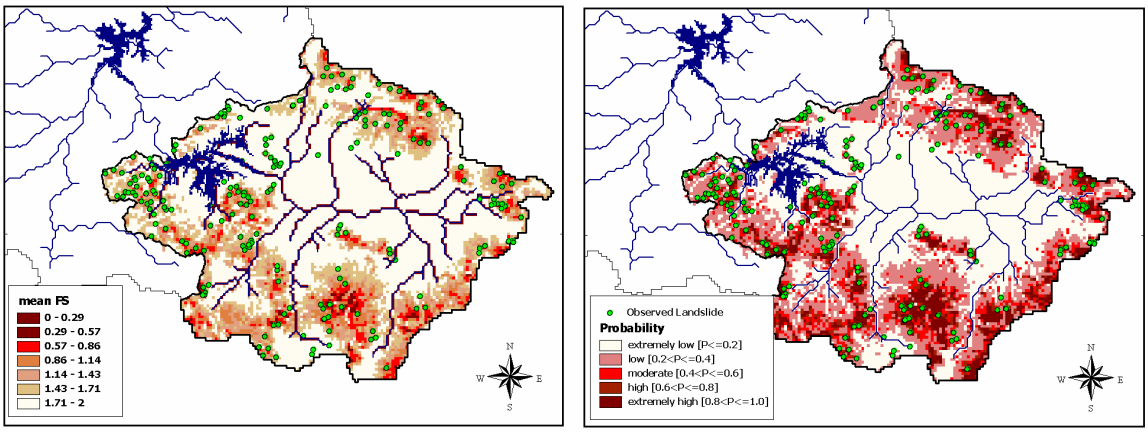

Fig. 11 Model output (mean FS and probability shallow landslide maps) for identification of the critical sub-catchment on the basis of landslide susceptibility area in the upper Citarum Catchment

8. Identification of the Critical Area of Soil Erosion and Shallow Landslide

According to the simulation results obtained for calibration period, the sub-catchment where soil erosion was serious can be identified. On the basis of higher annual sediment yield, the sediment budgets from each sub-catchment show that most sediment materials are generated and transported from the sub-catchments no. 8, 9, 2, and 1 (see Figures 9 & 10). The annual sediment yield in these sub-catchments were found to be critical. After arranging the critical sub-catchments in ascending order, considering the sediment fluxes and yields from each sub-catchment, priorities were fixed. Investment prioritization scenarios can be proposed to each of these sub-catchments. The sub-catchment that comes first (sub-catchment 8) is given the top priority for developing the management plan to reduce the surface soil erosion.

The results suggest that those critical sub-catchments with critical soil erosion also covered by the high probability landslide potential areas especially for the cases of sub-catchment no. 8 and 2 (Figure 11). In order to reduce the sediment yield due to surface soil erosion and slope instability disasters, sub-catchments no. 8 and 2 were selected and recommended to adopt the management measures.

Conclusions

The study confirmed that the proposed physically-based distributed hydrological-geotechnical model could accurately simulate runoff, sediment yield, and the spatial pattern of documented historical landslide events. From catchment-wide perspective, the study also revealed that all the sub-catchments in the study region do not all contribute to the water discharge, sediment yield, and slope instability occurrences. The model could identify the critical sub-catchments, which are major contributors of these variables.

As a further concern, linking the model and various best management practices (BMPs) scenario algorithms will be intended for design of control strategy in trapping and controlling sediment-runoff. It is addressed especially for ungauged sites of internal catchment with high sediment yields. Structural measures of BMPs are employed here: vegetative filter, wet pond, reservoir, and land use scenario.

Acknowledgment

This study was supported by the MEXT Coordination Fund for Promotion of Science and Technology, Japan Science and Technology Agency (PI: Prof. Kaoru Takara, DPRI, Kyoto Univ.).

References

Agus, F. and Wahyunto. (2003): Evaluation of flood mitigation function of several land use systems in selected areas of west java, Indonesia. Paper presented at Japan/OECD Expert Meeting on Land Conservation Indicators, 13-15 May, 2003, Kyoto, Japan.

Apip, Sayama, T., Tachikawa., Y. and Takara, K. (2008): Lumping of a physically-based distributed model for sediment runoff prediction in a catchment scale, *Annual Journal of Hydraulic Engineering, JSCE*, Vol. 52, pp 43-48.

Dickinson, W.T., Rudra, R.P., and Wall, G.J. (1990): Targeting remedial measures to control nonpoint source pollution. *Water Resource Bulletin*, AWRA, Vol. 26(3), pp. 499-507.

Foster, G.R. (1982): Modeling the erosion process. In *Hydrologic Modeling of Small Watersheds*. American Society of Agricultural Engineers, St. Joseph: pp 295-380.

Joyce, R.J., Janowiak, J.E., Arkin, P.A., and Xie, P. (2004): CMORPH: A method that produces global precipitation estimates from passive microwave and infrared data at high spatial and temporal resolution. *Journal of Hydrometeorology*, pp 5: 487-503.

Lin, W.T., Tsai, J.S., Lin, C.Y., and Huang, P.H. (2008): Assessing reforestation placement and benefit for erosion control: A case study on the Chi-Jia-Wan Stream, Taiwan. *Ecological Modelling*, Vol. 211, pp. 444-452.

Montgomery, D.R., and Dietrich, W.E. (1994): A physically-based model for the topographic control on shallow landsliding. *Water Resources Research*, Vol. 30, pp. 1153-1171.

Tachikawa, Y., Nagatani, G., and Takara, K. (2004): Development of stage-discharge relationship equation incorporating saturated-unsaturated flow mechanism. *Annual Journal of Hydraulic Engineering* (JSCE), pp 48: 7-12.

Takeuchi, K., Jayawardena, A.W., Takahashi, Y. (Eds.) (1995): Catalogue of rivers for Southeast Asia and the Pacific — Volume I," The UNESCO-IHP Regional Steering Committee for Southeast Asia and the Pacific, UNESCO-IHP Publication, pp 103-114.

Wu, P., Hamada, J., Mori, S., Tauhid, Y.I., Yamanaka, M.D., and Kimura, F. (2003): Diurnal variation of precipitable water over a mountainous area of Sumatera island. *Journal of Applied Meteorology*, pp 42:1107-1115.

Yang, C.T. (1996): Total load transport. In *Sediment Transport Theory and Practice*. The McGraw-Hill Companies, Inc: USA; pp 141-210.

未観測流域の土砂管理における優先投資区域決定のための土砂収支及び可能浅層地滑り範囲の空間分布の推定-インドネシアのチタラム川上流域を対象として

APIP*・寶馨・山敷庸亮・Agung Bagiawan IBRAHIM**

*京都大学工学研究科都市環境工学専攻
**インドネシア公共事業部門水資源研究センター

要　旨

流域の幾つかの地域は表土侵食や浅層地滑りによる大量の土壌損失の危険に曝されている。土壌損失を効果的に制御するために流域のこれらの地域において最善のマネージメント手法の実施が必要とされている。流域管理計画の効果的・効率的な実施のためにこれらの危険地域の同定が必要不可欠である。この研究では流域上流域 (2,310 km^2) を対象に物理即に基づく分布型の水文地質モデルを開発し，有効な管理計画を実施するために必要な土砂災害危険地域（サブ流域スケール）の同定のためのツールとして用いる。このモデルは二つの要素，すなわち降雨滴と表面流出による土砂の分離を考慮した斜面土砂流出モデルと確率斜面不安定性予測モデルからなる。2001 年～2004 年の日流量と土砂生産高データ及び 1985 年～2008 年地滑り記録がモデルの検証及び適用に使われた。土砂生産高率及び予測浅層地滑り確率の空間分布にもとづいて危険なサブ流域が同定された。これらにより提案した分布型モデルが流域管理の目的で土砂災害危険地域の同定に適用可能である事が示された。

キーワード：土砂管理，土壌侵食，斜面不安定性，チタラム流域